On the geometry of fracture and frustration

Koning, V.

Part III

FRACTURE OF CURVED SOLIDS

In this final part we turn our attention from confined liquid crystals to geometrically frustrated solids. The curvature of two-dimensional solids which are forced to adopt a certain shape, is a source of stress. We study the effects of the stress on the fracture mechanics of such solids. We find that the curvature can both decrease or increase the critical length at which the crack starts growing depending on the location and orientation of the crack, thus both stimulating and inhibiting the onset of crack growth. Finally, the non-uniform stress generates curved crack trajectories.

5

ONSET OF CRACK GROWTH

5.1 LINEAR ELASTIC FRACTURE MECHANICS

The first and foremost one should realise when studying how things break is that fracture occurs through the propagation of one or more cracks [59]. It is exceptionally rare that materials break because a series of bonds extending from one end of the sample to the other end all break simultaneously. A real solid is not so perfect and contains flaws at which the stresses are focussed: near the tip of a crack the stresses and strains become very large. As a consequence, the material around the tip will fail and the crack will propagate. If the material behaves linear elastically, the stress tensor σ_{ij} at a distance r from the crack tip which is assumed to be small compared to the crack length a reads [8, 83, 116]

$$\sigma_{ij} = \frac{K_I}{\sqrt{2\pi r}} f_{ij}^{I}(\theta) + \frac{K_{II}}{\sqrt{2\pi r}} f_{ij}^{II}(\theta), \tag{178}$$

Close to the crack tip the stress is not infinite as is suggested by the inverse square root of r in eq. (178), but finite. The small region in which plastic deformations occur is called the process zone. If the radius of this zone, r_p, is small compared to the crack length – called an assumption of small scale yielding – eq. (178) describes the stresses in the annulus $r_p \ll r \ll a$ well. The sub- and superscripts I and II in eq. (178) refer to the modes of fracture, which are displayed in Fig. 45. In two dimensions, there are two symmetry modes of fracture, namely an opening mode (traditionally labelled as mode I) and a sliding or shearing mode (traditionally labelled as mode II). For a horizontally aligned crack (*i.e.* in the x direction), in mode I vertical displacements are anti-symmetric in reflection about the x-axis ($u_y(x,-y) = -u_y(x,y)$) and horizontal displacements are symmetric ($u_x(x,-y) = u_x(x,y)$). In mode II it is the other way around: vertical displacements are symmetric ($u_y(x,-y) = u_y(x,y)$) and horizontal displacements are anti-symmetric ($u_x(x,-y) = -u_x(x,y)$). Under general loading conditions, the problem can be decomposed into these two modes.

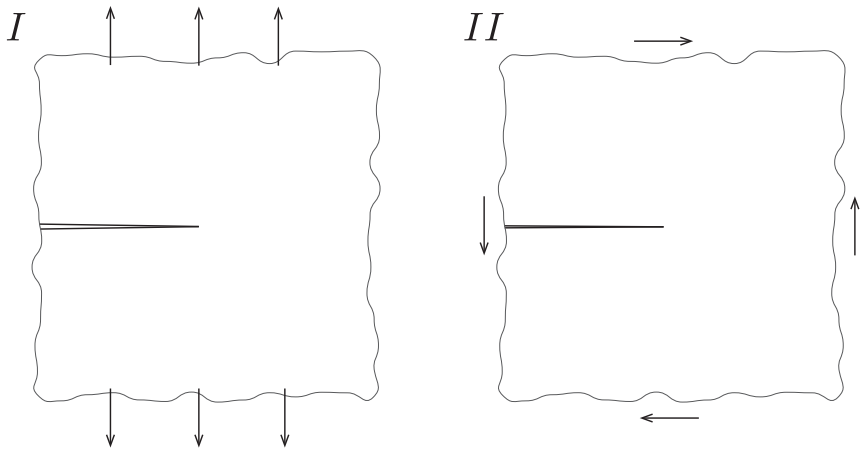

Figure 45: *Left panel:* Schematic of mode I fracture. *Right panel:* Schematic of mode II fracture.

The functions functions f_{ij}^{I} and f_{ij}^{II} are universal, meaning that they neither depend on loading conditions nor geometry. Thus, f_{ij}^{I} and f_{ij}^{II} are the same for cracks in the bulk and at the edge, for disk-shaped samples, strips, and infinite domains. They only depend on the polar angle θ (where the location of the tip is taken as the origin, see Fig. 46) and read:

$$f_{rr}^{I} = -\frac{1}{4}\cos\left(\frac{\theta}{2}\right) + \frac{5}{4}\cos\left(\frac{3\theta}{2}\right), \tag{179}$$

$$f_{\theta\theta}^{I} = \frac{3}{4}\cos\left(\frac{\theta}{2}\right) + \frac{1}{4}\cos\left(\frac{3\theta}{2}\right), \tag{180}$$

$$f_{r\theta}^{I} = \frac{1}{4}\sin\left(\frac{\theta}{2}\right) + \frac{1}{4}\sin\left(\frac{3\theta}{2}\right), \tag{181}$$

and

$$f_{rr}^{II} = -\frac{5}{4}\sin\left(\frac{\theta}{2}\right) + \frac{3}{4}\sin\left(\frac{3\theta}{2}\right), \tag{182}$$

$$f_{\theta\theta}^{II} = -\frac{3}{4}\sin\left(\frac{\theta}{2}\right) - \frac{3}{4}\sin\left(\frac{3\theta}{2}\right), \tag{183}$$

$$f_{r\theta}^{II} = \cos\left(\frac{\theta}{2}\right) + 3\cos\left(\frac{3\theta}{2}\right). \tag{184}$$

Eqs. (178)-(184)) follow from Williams' asymptotic analysis [110]: solving the equilibrium equations in the vicinity of the crack tip with the crack modelled as a slit with two edges that are closed in the reference state but which could open up once loading is applied. The only variables in eq. (178) which are not universal,

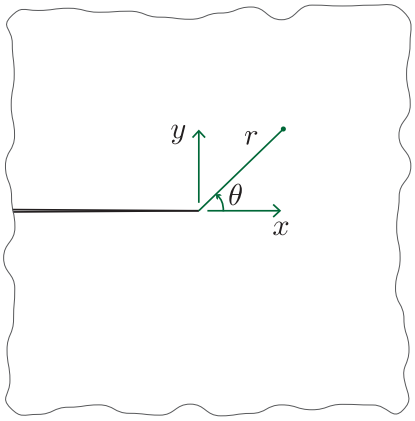

Figure 46: Schematic of the crack tip coordinates for a crack aligned in the x-direction.

are the prefactors K_I and K_{II}. These prefactors are called the stress intensity factors (of mode I and mode II, respectively), because they characterise the strength of the stress singularity. All information about loading, crack length and the shape of the sample reduce to this one quantity, thus making it one of the most important concepts in linear elastic fracture mechanics. Indeed, it is believed to determine the onset and direction of crack growth. For instance, a mode I crack will start to propagate if K_I exceeds a critical value, K_c. The critical vale for the stress intensity factor, K_c, which determines the onset of crack growth, is often referred to as the fracture toughness and it is a material property. If the crack growth is quasistatic, the growth also comes to a halt if the stress intensity factor drops below the critical value again. We call this stable crack growth. The growth is unstable if the crack continues propagating till the material fails. Several theories for mixed-mode fracture exist, of which one of them is the criterion of maximum circumferential, or hoop, stress [116]. This postulates that the pre-existing crack will grow in the direction θ_c in which $\sigma_{\theta\theta}(\theta)$ is the largest, thus satisfying

$$\frac{\partial \sigma_{\theta\theta}}{\partial \theta}|_{\theta=\theta_c} = 0, \quad \frac{\partial^2 \sigma_{\theta\theta}}{\partial \theta^2}|_{\theta=\theta_c} < 0 \tag{185}$$

Applying this criterion to eqs. (178)-(184) yields the kink angle

$$\theta_c = 2 \arctan\left(\frac{-2\eta}{1+\sqrt{1+8\eta^2}}\right), \tag{186}$$

where $\eta \equiv K_{II}/K_I$. A propagating crack will eventually turn its orientation such as to be in mode I and experience a maximum tensile stress. The condition for the onset of crack growth in this theory of mixed-mode fracture is that the intensity factor in the direction of maximum circumferential stress exceeds a critical value, which is assumed to be the same as for pure mode I loading:

$$\sigma_{\theta\theta}\left(\theta_c\right)\sqrt{2\pi r} > K_c. \tag{187}$$

Finally, besides crack growth criteria, the stress intensity factors also yield the shape of the crack tip opening. The displacement fields in the vicinity of the crack tip are obtained from the stress fields given by eqs. (178)-(184):

$$u_r^I = K_I \frac{1+\nu}{Y}\sqrt{\frac{r}{2\pi}}\left[\left(\frac{5}{2} - 4\frac{\nu}{1+\nu}\right)\cos\left(\frac{\theta}{2}\right) - \frac{1}{2}\cos\left(\frac{3\theta}{2}\right)\right], \tag{188}$$

$$u_\theta^I = K_I \frac{1+\nu}{Y}\sqrt{\frac{r}{2\pi}}\left[-\left(\frac{7}{2} - 4\frac{\nu}{1+\nu}\right)\sin\left(\frac{\theta}{2}\right) + \frac{1}{2}\sin\left(\frac{3\theta}{2}\right)\right], \tag{189}$$

and

$$u_r^{II} = K_I \frac{1+\nu}{Y}\sqrt{\frac{r}{2\pi}}\left[\left(-\frac{5}{2} - 4\frac{\nu}{1+\nu}\right)\sin\left(\frac{\theta}{2}\right) + \frac{3}{2}\sin\left(\frac{3\theta}{2}\right)\right], \tag{190}$$

$$u_\theta^{II} = K_I \frac{1+\nu}{Y}\sqrt{\frac{r}{2\pi}}\left[-\left(\frac{7}{2} - 4\frac{\nu}{1+\nu}\right)\cos\left(\frac{\theta}{2}\right) + \frac{3}{2}\cos\left(\frac{3\theta}{2}\right)\right], \tag{191}$$

where Y is Young's modulus and ν is Poisson's ratio. For a pure mode I crack, the vertical displacement at the crack edges (*i.e.* $\theta = \pm\pi$) reads

$$u_y\left(r, \pm\pi\right) = -u_\theta\left(r, \pm\pi\right) = \pm\frac{4K_I}{Y}\sqrt{\frac{r}{2\pi}}. \tag{192}$$

Hence, the shape of the crack tip is parabolic.

5.2 CRACKS IN A GAUSSIAN BUMP

5.2.1 *Problem formulation*

In this chapter we will study cracks in two-dimensional curved solids. Examples of two-dimensional curved solids are colloidal particles at a fluid-fluid interface, viral shells or plates, *e.g.* in aircraft

structures, where out-of plane deflection may be large compared to the plate thickness [108, 33, 117]. Besides the in-plane fracture modes introduced in the previous section, there are bending modes that we will discard in our analysis [111, 89, 33, 117]. We will focus on the effects of the in-plane stresses generated by the curvature. As pointed out by Hui et al., in curved plates the near tip stress fields will display the same singular behaviour as in eq. (178) [33, 117]. However, the values of the stress intensity factors are affected by the curvature. In turn, this influences the onset and direction of growth of pre-existing cracks.

5.2.2 *The Gaussian bump*

The surface that we will choose to study the effects of the geometric frustration on cracks is the gaussian bump (Fig. 47), whose height profile reads

$$h(\mathbf{x}) = \alpha x_0 \exp\left(-\rho^2/2\right), \tag{193}$$

where x_0 is a measure of the width of bump, $\rho = |\mathbf{x}|/x_0$ is the normalised radial coordinate, and $\alpha = h(0)/x_0$ is the aspect ratio of the bump. This surface has several convenient and interesting

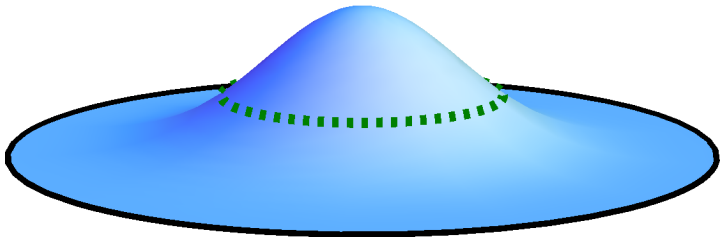

Figure 47: Schematic of a Gaussian bump. The circle $\rho = 1$, indicating the width of the bump, is drawn in dashed green. The circle $\rho = R/x_0$, which is the edge of the disk, is drawn in black.

features. First, it has a flat counterpart (unlike *e.g.* a sphere), such that one can tune α continuously from zero to a finite value. Second, it has a varying Gaussian curvature with regions of positive

and negative curvature. The curvature is positive for $\rho < 1$ and negative for $\rho > 1$. Indeed, from eq. (75) we find [107]

$$G(\rho) = \frac{\alpha^2}{x_0^2} \exp\left(-\rho^2\right) \frac{1-\rho^2}{\left(1+\alpha^2\rho^2 \exp\left(-\rho^2\right)\right)^2} \tag{194}$$

$$\approx \frac{\alpha^2}{x_0^2} \exp\left(-\rho^2\right)\left(1-\rho^2\right). \tag{195}$$

The latter approximation is valid, because we are working in the regime of small α^2. Finally, we consider the origin of the Gaussian bump to be located at the centre of the disk of radius R. If one considers samples much smaller than the width of the bump $R \ll x_0$, then $G \to \alpha^2/x_0^2$ and so the Gaussian bump reduces to a spherical cap with radius of curvature of x_0/α.

5.2.3 *Decomposing the problem*

We need to solve for the equilibrium equations of linear elasticity with an infinitely narrow cut (representing the crack) in a Gaussian bump, possibly under external loading. This external loading is usually applied at the boundary of the sample, though in principle could also be applied at the crack edges. We will decompose the problem of a crack with stress-free edges in a Gaussian bump loaded at the boundary into two other problems, called A and B. The first of these two problems is finding the stress field, $\sigma_{ij}^G(\mathbf{x})$, prior to the introduction of the crack, due to curvature and external loading only. Next, in problem B, we solve for the stress field, $\sigma_{ij}^0(\mathbf{x})$, for a crack whose edges are loaded, but in which there is neither curvature nor loading at the boundary of the sample. The traction, $\mathbf{p}$, applied at the crack edges is such that it cancels the tractions in the first problem, *i.e.* the traction on the top crack edge is

$$p_i = -\sigma_{ij}^G \nu_j, \tag{196}$$

with $\boldsymbol{\nu}$ the normal vector of the top crack edge, and the traction loading on the bottom crack edge is equal but opposite. Thus, the stresses generated by the curvature serve as traction on the crack edges. Superposing the stress fields in problem A with the stress fields in problem B, $\sigma_{ij}(\mathbf{x}) = \sigma_{ij}^G(\mathbf{x}) + \sigma_{ij}^0(\mathbf{x})$, solves the initial problem (see Fig. 48). It satisfies the equilibrium equations (eq.

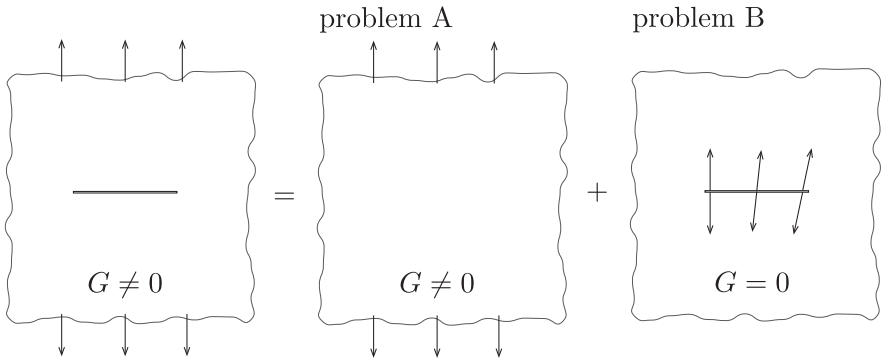

Figure 48: The solution of the problem on the left hand side of this schematic equation is obtained by superposing the stress fields in A and B. In A there is geometric frustration due to the nonzero curvature, but no crack. In B there is no curvature, but there is a crack whose edges are loaded such as to cancel the stresses generated in A at the crack location. In B, the arrows representing the forces at the crack edge are drawn non-vertical intentionally, because generally $\sigma^G_{xy} \neq 0$ and hence there could be a shear force.

(39)),

$$\partial_i \sigma_{ij} = \partial_i \sigma^G_{ij} + \partial_i \sigma^0_{ij} = 0, \tag{197}$$

as well as the equation for the Airy stress function (eq. 75)

$$\frac{1}{Y}\partial^4 \chi = \frac{1}{Y}\partial^4 \chi^G + \frac{1}{Y}\partial^4 \chi^0 = -G. \tag{198}$$

Moreover, conditions at both the boundary of the sample and at the crack edge are correct. In the absence of any curvature, this decomposition reduces to the usual equivalence of crack face loading and far field loading. Since σ^G does not contain any singularity, the stress intensity factors of σ^0 are equal to the stress intensity factors of the full solution σ.

5.2.4 *Stress fields in the absence of cracks*

The first problem involves solving for the stresses as a result of Gaussian curvature only, prior to the introduction of the crack. Firstly, we will take the circular boundary of the disk traction-

free. For the stress components $\sigma^G_{\rho\rho}(\rho)$ and $\sigma^G_{\rho\phi}(\rho)$ evaluated at the boundary we thus have

$$p_\rho = \sigma^G_{\rho\rho}(R/x_0) = 0, \tag{199}$$
$$p_\phi = \sigma^G_{\rho\phi}(R/x_0) = 0. \tag{200}$$

Due to rotational symmetry $\sigma^G_{\rho\phi} = 0$ [107]. The trace of the stress tensor, however, reads [107]

$$\sigma^G_{\rho\rho} + \sigma^G_{\phi\phi} = \frac{\alpha^2}{4} Y \left(\frac{x_0^2}{R^2} \exp\left(-\frac{R^2}{x_0^2} \right) - \frac{x_0^2}{R^2} + \exp\left(-\rho^2\right) \right). \tag{201}$$

From this starting point we obtain $\sigma^G_{\rho\rho}$ and $\sigma^G_{\phi\phi}$. Again, employing rotational symmetry the force-balance in the ρ direction reads

$$\rho \frac{\partial \sigma^G_{\rho\rho}}{\partial \rho} + \sigma^G_{\rho\rho} - \sigma^G_{\phi\phi} = 0. \tag{202}$$

Substituting eq. (201) to eliminate $\sigma^G_{\phi\phi}$ yields a differential equation for $\sigma^G_{\rho\rho}$ whose solution is

$$\sigma^G_{\rho\rho} = \frac{C}{\rho^2} - \frac{\alpha^2 Y}{8\rho^2} \exp\left(-\rho^2\right) + \frac{\alpha^2 Y}{8} \frac{x_0^2}{R^2} \left[\exp\left(-\frac{R^2}{x_0^2} \right) - 1 \right]. \tag{203}$$

Demanding that the stress is finite at the origin sets the integration constant $C = Y\alpha^2/8$. We thus find

$$\sigma^G_{\rho\rho} = \frac{\alpha^2}{8} Y \left(\rho^{-2} \left[1 - \exp\left(-\rho^2\right) \right] + \frac{x_0^2}{R^2} \left[\exp\left(-\frac{R^2}{x_0^2} \right) - 1 \right] \right), \tag{204}$$

for the radial stress component. Substituting $\sigma^G_{\rho\rho}$ back into eq. (201) yields for the azimuthal component

$$\sigma^G_{\phi\phi} = \frac{\alpha^2}{8} Y \left(\rho^{-2} \left[\exp\left(-\rho^2\right) - 1 \right] + 2\exp\left(-\rho^2\right) + \frac{x_0^2}{R^2} \left[\exp\left(-\frac{R^2}{x_0^2} \right) - 1 \right] \right). \tag{205}$$

These stress components are plotted as a function of ρ in Fig. 49a. If instead of traction-free boundary conditions (eqs. (199)-(200)), we apply a radial force of magnitude P,

$$p_\rho = P, \tag{206}$$
$$p_\phi = 0, \tag{207}$$

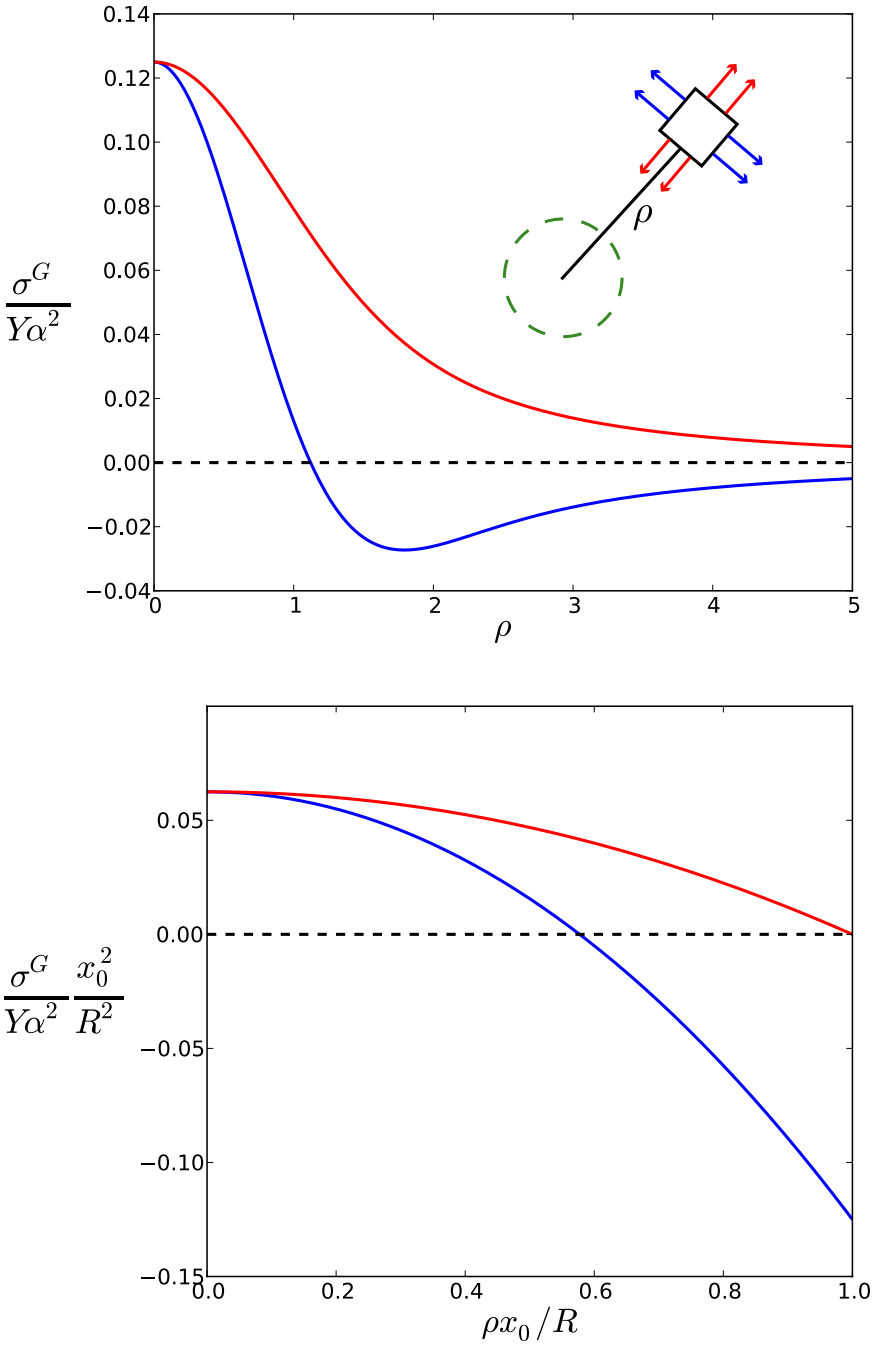

Figure 49: Stress components $\sigma^G_{\rho\rho}$ (red) and $\sigma^G_{\phi\phi}$ (blue) for $P = 0$ and $R/x_0 \to \infty$ (*top panel*), $R/x_0 = 0.01$ (*bottom panel*) as a function of the rescaled radius. *Inset:* Schematic of $\sigma^G_{\rho\rho}$ and $\sigma^G_{\phi\phi}$ indicated by red and blue arrows, respectively. The bump is indicated by the green dashed circle $\rho = 1$.

we can simply superpose a uniform stress field $\sigma_{\rho\rho} = P$ and $\sigma_{\phi\phi} = P$ to the obtained expression for σ_{ij}:

$$\sigma^G_{\rho\rho} = \frac{\alpha^2}{8} Y \left(\rho^{-2} \left[1 - \exp\left(-\rho^2\right) \right] + \frac{x_0^2}{R^2} \left[\exp\left(-\frac{R^2}{x_0^2} \right) - 1 \right] \right) + P, \tag{208}$$

$$\sigma^G_{\phi\phi} = \frac{\alpha^2}{8} Y \left(\rho^{-2} \left[\exp\left(-\rho^2\right) - 1 \right] + 2\exp\left(-\rho^2\right) + \frac{x_0^2}{R^2} \left[\exp\left(-\frac{R^2}{x_0^2} \right) - 1 \right] \right) + P. \tag{209}$$

In an infinite medium ($R \to \infty$), the non-vanishing stress components reduce to

$$\sigma^G_{rr} = \frac{\alpha^2}{8} Y \rho^{-2} \left(1 - \exp\left(-\rho^2\right) \right) + P, \tag{210}$$

$$\sigma^G_{\phi\phi} = \frac{\alpha^2}{8} Y \left(\rho^{-2} \left[\exp\left(-\rho^2\right) - 1 \right] + 2\exp\left(-\rho^2\right) \right) + P. \tag{211}$$

Finally, in the spherical cap regime ($R \ll x_0$) we find (Fig. 49b)

$$\sigma^G_{\rho\rho} \approx \frac{\alpha^2}{16} Y \left(R^2/x_0^2 - \rho^2 \right) + P, \tag{212}$$

$$\sigma^G_{\phi\phi} \approx \frac{\alpha^2}{16} Y \left(R^2/x_0^2 - 3\rho^2 \right) + P. \tag{213}$$

The azimuthal stress is compressive for $|\mathbf{x}| > R/\sqrt{3} \approx 0.58R$ for $P = 0$.

5.2.5 *Results for small center cracks*

Now that we have solved for the stresses prior to the introduction of the crack, we can calculate the stress intensity factors by means of weight function. The stress intensity factor is an integral over the length of the crack, which we define as $2a$ for a crack in the bulk. The product of the applied traction at the crack edge with the weight function, $m(x, a)$, comprises the integrand:

$$K_I = \int_{-a}^{a} m(\xi, a)\, p_y(\xi)\, d\xi, \tag{214}$$

$$K_{II} = \int_{-a}^{a} m(\xi, a)\, p_x(\xi)\, d\xi. \tag{215}$$

The weight function can be viewed as the stress intensity factor for a force dipole at x, *i.e.* $p_y(\xi) = \delta(\xi - x)$ for mode I or $p_x(\xi) = \delta(\xi - x)$ for mode II. The weight function depends on the length of the crack, but also on the location of the applied traction and diverges at the tip. For instance, the weight function for the tip at $x = a$ of a crack in an infinite plane is

$$m(x, a) = \frac{1}{\sqrt{\pi a}} \sqrt{\frac{a + \xi}{a - \xi}}. \tag{216}$$

The stress intensity factors for such a centre crack in a Gaussian bump are thus

$$K_I = \frac{1}{\sqrt{\pi a}} \int_{-a}^{a} d\xi \sqrt{\frac{a + \xi}{a - \xi}}\, \tilde{\sigma}^G_{yy}(\xi, 0), \tag{217}$$

$$K_{II} = \frac{1}{\sqrt{\pi a}} \int_{-a}^{a} d\xi \sqrt{\frac{a + \xi}{a - \xi}}\, \tilde{\sigma}^G_{xy}(\xi, 0), \tag{218}$$

where $\tilde{\sigma}^G_{ij}(x, y)$ is the stress due to geometric frustration only. The origin of the xy coordinate system is at the middle of the crack.[1] If the crack size is small enough compared to the length scale over which the stresses vary, *i.e.*

$$a \left| \partial_x \tilde{\sigma}^G_{iy} \right| \ll \tilde{\sigma}^G_{iy}, \tag{219}$$

it is legitimate to take σ^G_{iy} out of the integrand and we obtain the following result

$$K_I = \frac{\tilde{\sigma}^G_{yy}(0, 0)}{\sqrt{\pi a}} \int_{-a}^{a} d\xi \frac{a + \xi}{\sqrt{a^2 - \xi^2}} = \sqrt{\pi a} \tilde{\sigma}^G_{yy}(0, 0), \tag{220}$$

$$K_{II} = \frac{\tilde{\sigma}^G_{xy}(0, 0)}{\sqrt{\pi a}} \int_{-a}^{a} d\xi \frac{a + \xi}{\sqrt{a^2 - \xi^2}} = \sqrt{\pi a} \tilde{\sigma}^G_{xy}(0, 0). \tag{221}$$

This result holds irrespective of the details of the shape of the surface. For a Gaussian bump with a crack that is aligned radially, eqs. (220) and (221) reduce to

$$K_I = \sqrt{\pi a}\, \sigma^G_{\phi\phi}(\rho^*), \tag{222}$$

$$K_{II} = 0, \tag{223}$$

1 The tilde is there to distinguish it from σ^G_{ij} which generally is a function of ρ, and thus, although it describes the same physical quantity, is a different function of its arguments.

where ρ^* is the distance to the crack from the centre of the bump. Since K_{II} the crack will grow radially if $K_I > K_c$. For the bump this implies that the critical length, a_c, at which radial cracks will grow is

$$a_c = \frac{K_c^2}{\pi \left(\sigma_{\phi\phi}^G \left(\rho^*\right)\right)^2}. \tag{224}$$

We plot this quantity in Fig. 50 for several aspect ratios of the bump in an infinite plane (*i.e.* $R \to \infty$)) and $P = 0.01Y$. We

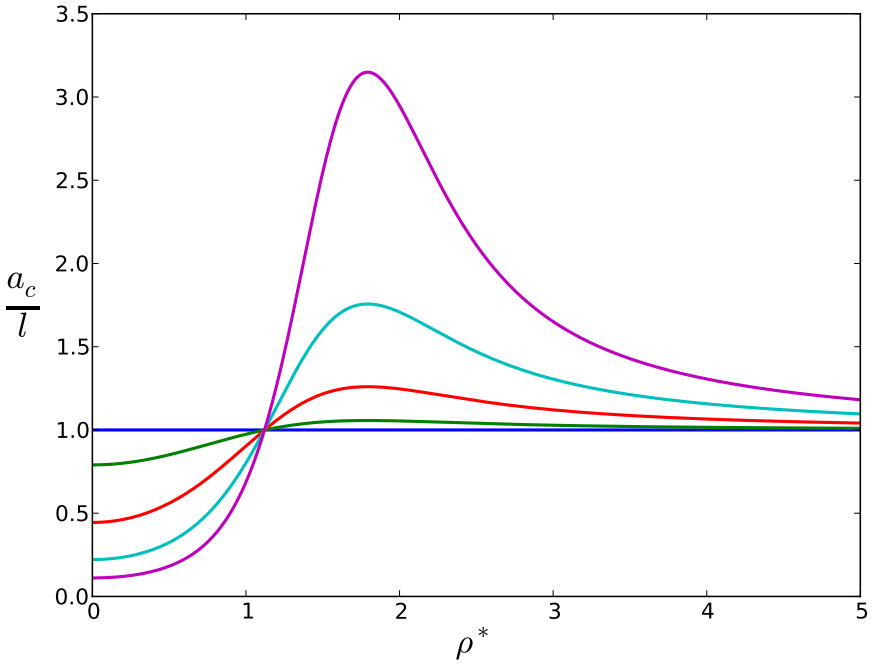

Figure 50: Normalised critical length of the small straight crack in the radial direction versus normalised radial distance of the location of the crack for $P = 0.01Y$ and aspect ratios $\alpha = 0$ (blue), $\alpha = 0.1$ (green), $\alpha = 0.2$ (red), $\alpha = 0.3$ (cyan) and $\alpha = 0.4$ (magenta).

have normalised a_c by the length, l, at which a crack under 1% strain (*i.e.* $P = 0.01Y$) would grow in the flat case (*i.e.* $\alpha = 0$). The critical size is smallest if the crack is located at the top of the bump ($\rho^* = 0$), where $\sigma_{\phi\phi}^G$ has its maximum. The critical crack length is largest at $\rho^* \approx 1.8$, where $\sigma_{\phi\phi}^G$ has its minimum. Since $\sigma_{\phi\phi}^G$ flips sign at $\rho^* \approx 1.1$, the normalised critical crack length a_c/l crosses unity for $\rho^* \approx 1.1$. For cracks located at radial distances smaller than this value, $a_c/l < 1$ and the curvature thus stimulates crack growth. On the other hand, if the crack is located sufficiently

far from the bump, $a_c/l > 1$ and the crack growth is suppressed. It should be noted that for cracks located such that we find $K_1 < 0$ (signalled by a divergence of a_c), the stress field is not given by eqs. (178)-(184)), because the crack edges would have to interpenetrate. As can be seen from eq. (192), $K_1 < 0$ would give $u_y(r, \pi) < 0$ on the top edge and $u_y(r, \pi) > 0$ on the bottom edge. In practice, crack closure or bulging occurs [8]. If α increases (or P decreases) further there will be an annular region for which this occurs.

For a small crack in the azimuthal direction rather than radial direction, we find

$$K_I = \sqrt{\pi a}\, \sigma^G_{\rho\rho}(\rho^*), \tag{225}$$

$$K_{II} = 0. \tag{226}$$

and the critical crack length is given by

$$a_c = \frac{K_c^2}{\pi \left(\sigma^G_{\rho\rho}(\rho^*)\right)^2}. \tag{227}$$

For small azimuthal cracks, the curvature suppresses the crack growth independently of the value of ρ^*, as is shown in Fig. 51, because $\sigma^G_{\rho\rho} > 0$. The critical crack length is smaller in the presence of curvature than in the absence of curvature, no matter where the azimuthal crack is located.

Next we will consider the general case in which the orientation of the crack makes an angle β with the radial direction. The traction at the crack edge reads

$$p_y \approx \tilde{\sigma}^G_{yy}(0,0) = \sigma^G_{\rho\rho}(\rho^*)\sin^2\beta + \sigma^G_{\phi\phi}(\rho^*)\cos^2\beta, \tag{228}$$

$$p_x \approx \tilde{\sigma}^G_{xy}(0,0) = \left(\sigma^G_{\phi\phi}(\rho^*) - \sigma^G_{\rho\rho}(\rho^*)\right)\sin\beta\cos\beta. \tag{229}$$

The stress intensity factors are therefore

$$K_I = \sqrt{\pi a}\left(\sigma^G_{\rho\rho}(\rho^*)\sin^2\beta + \sigma^G_{\phi\phi}(\rho^*)\cos^2\beta\right), \tag{230}$$

$$K_{II} = \sqrt{\pi a}\left(\sigma^G_{\phi\phi}(\rho^*) - \sigma^G_{\rho\rho}(\rho^*)\right)\sin\beta\cos\beta. \tag{231}$$

For the radial and azimuthal crack ($\beta = 0$ and $\beta = \pi/2$, respectively) we recover $K_{II} = 0$, and there will thus not be a kink. However, for intermediate values of α, *i.e.* $\beta \pmod{\pi/2} \neq 0$, the mode II stress intensity factor does not vanish. Therefore, if the crack does grow, it will grow in a different direction than the direction of the pre-existing crack. This kink angle can be calculated

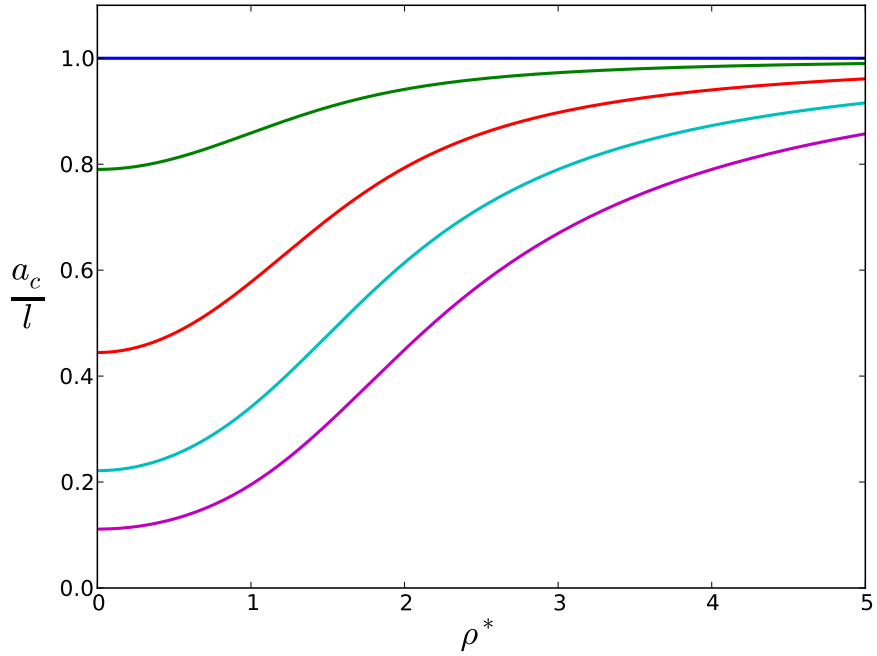

Figure 51: Normalised critical length of the small straight crack in the azimuthal direction versus normalised radial distance of the location of the crack for $P = 0.01Y$ and aspect ratios $\alpha = 0$ (blue), $\alpha = 0.1$ (green), $\alpha = 0.2$ (red), $\alpha = 0.3$ (cyan) and $\alpha = 0.4$ (magenta).

with the maximum hoop stress criterium (eq. (186)) and is plotted for $\beta = \pi/4$ in the top panel of Fig. 52 as a function of ρ for several values of α. The sign of the kink angle is determined by the sign of K_{II}. If K_{II} is positive (negative), that is, η is positive (negative), assuming P is large enough to prevent a nonphysical negative K_I, then θ_c is negative (positive). The sign of θ_c is independent of the crack location, because $\sigma^G_{\rho\rho} \geq \sigma^G_{\phi\phi}$ for all ρ^*, but is depending on the value for β, as is illustrated in the top panels of Fig. 53 and Fig. 54 for $\rho^* = 2$ and $\rho^* = 0.5$. We find $K_{II} < 0$ (or $K_{II} > 0$) for $0 < \beta \pmod{\pi} < \frac{\pi}{2}$ (or $\frac{\pi}{2} < \beta \pmod{\pi} < \pi$) and so $\theta_c > 0$ (or $\theta_c < 0$). For all values of β this implies that the crack direction will be corrected toward the azimuthal direction. The top panel of Fig. 53 also shows that the value for which the kink angle is the largest (which is where the ratio of the mode II and mode I stress intensity factors is the largest) occurs at a value for β which is typically somewhat smaller than $\pi/4$. Since the loading is mixed mode, the stress that enters in the formula

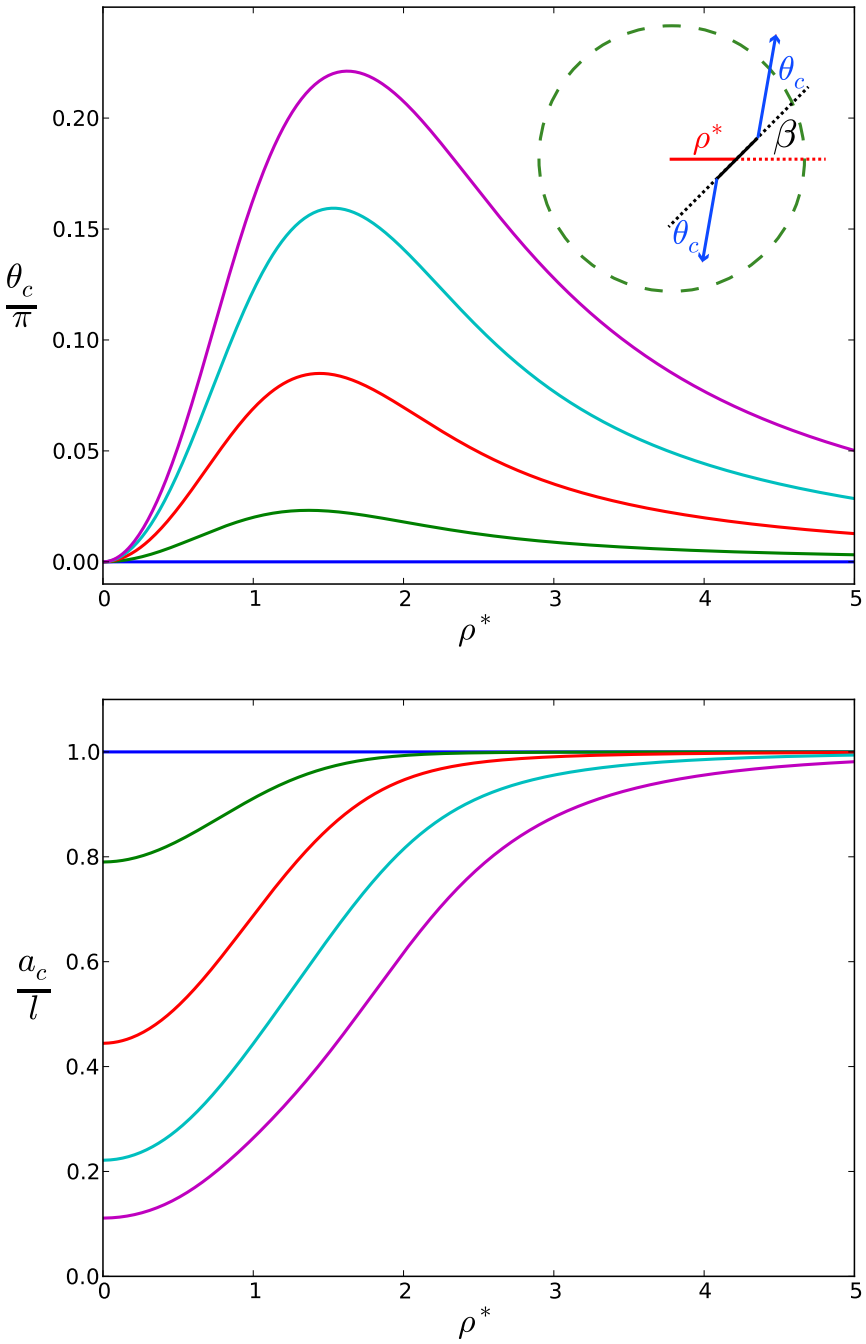

Figure 52: Kink angle (*top panel*) and normalised critical length of the small straight crack (*bottom panel*) versus normalised radial distance of the location of the crack for $\beta = \pi/4$ and $P = 0.01Y$ and aspect ratios $\alpha = 0$ (blue), $\alpha = 0.1$ (green), $\alpha = 0.2$ (red), $\alpha = 0.3$ (cyan) and $\alpha = 0.4$ (magenta). *Inset*: Schematic with graphical definitions of ρ^*, β and θ_c.

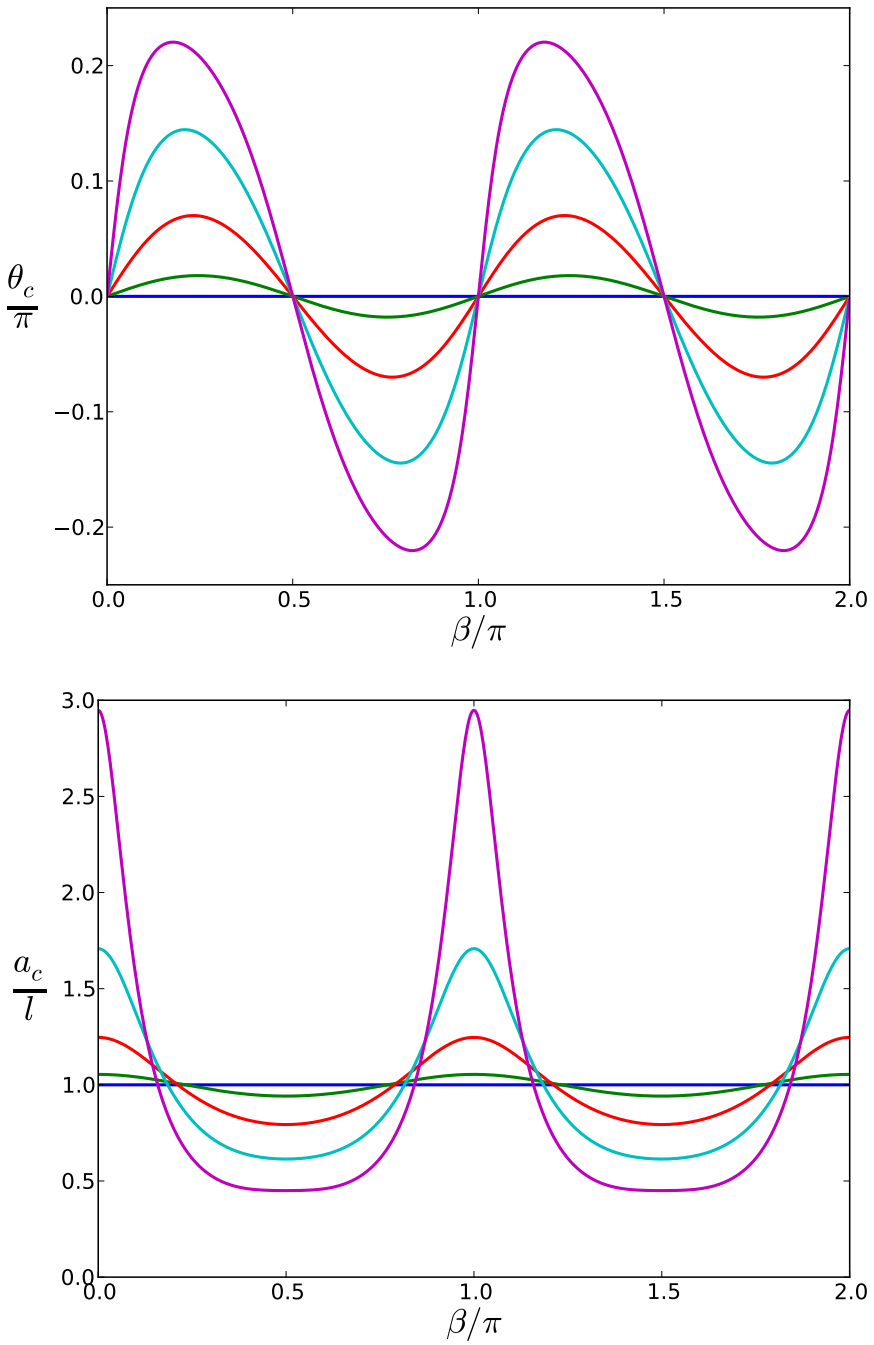

Figure 53: Kink angle (*top panel*) and normalised critical length of the small straight crack (*bottom panel*) versus the orientation of the crack for $\rho^* = 2$ and $P = 0.01Y$ and aspect ratios $\alpha = 0$ (blue), $\alpha = 0.1$ (green), $\alpha = 0.2$ (red), $\alpha = 0.3$ (cyan) and $\alpha = 0.4$ (magenta).

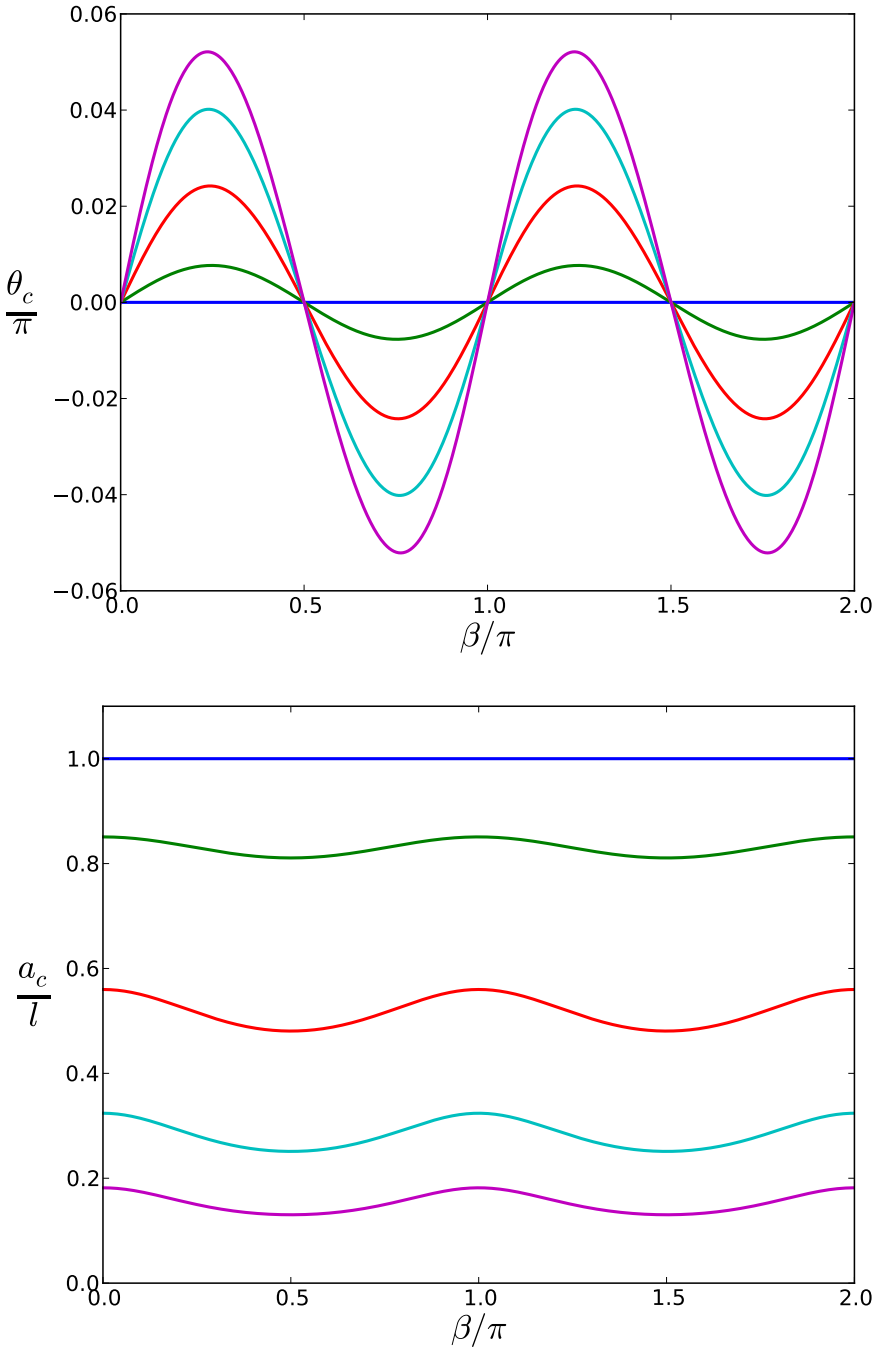

Figure 54: Kink angle (*top panel*) and normalised critical length of the small straight crack (*bottom panel*) versus the orientation of the crack for $\rho^* = 0.5$ and $P = 0.01Y$ and aspect ratios $\alpha = 0$ (blue), $\alpha = 0.1$ (green), $\alpha = 0.2$ (red), $\alpha = 0.3$ (cyan) and $\alpha = 0.4$ (magenta).

for the critical crack length is the circumferential stress (evaluated for $\theta = \theta_c$ in eq. (178)), and eq. (187) gives

$$a_c = \frac{K_c^2}{\pi \left(\sigma_{yy}^G \left(\rho^* \right) f_{\theta\theta}^I \left(\theta_c \right) + \sigma_{xy}^G \left(\rho^* \right) f_{\theta\theta}^{II} \left(\theta_c \right) \right)^2}. \tag{232}$$

We again plot the critical size as a function of crack location in the bottom panel of Fig. 52, now for $\beta = \pi/4$, and as a function of β in the bottom panel of Fig. 53 for $\rho^* = 2$. The latter shows that the curvature suppresses crack growth the most when the crack is oriented radially (*i.e.* $\beta = 0,\ \pi$), and stimulates crack growth the most when the crack is aligned azimuthally (*i.e.* $\beta = \pi/2,\ 3\pi/2$). For $\rho^* \lesssim 1.1$, the curvature stimulates the crack growth irrespective of the orientation of the crack, as is shown in the bottom panel of Fig. 54 for $\rho^* = 0.5$.

5.3 CONCLUSIONS

The critical length of the crack can both be enhanced or diminished by geometry-induced stress, in contrast to uniformly applied outward force at the boundary of the disk, which always stimulates crack growth. For a radial crack in a Gaussian bump, the critcal length decreases for cracks located at distances to the top smaller than $\rho^* \approx 1.1$. For radial cracks located at $\rho^* \gtrsim 1.1$ the critical length is increased by the curvature. This effect is strongest when $\rho^* \approx 1.8$. The critical size of an azimuthally oriented crack is decreased by the curvature irrespective of position. In addition to the critical size, also the kink angle depends on the location and orientation of the crack. The pre-existing crack will start to grow in a direction with a larger azimuthal component.